Blocking over the South Pacific and Rossby Wave Propagation

JAMES A. RENWICK AND MICHAEL J. REVELL

National Institute of Water and Atmospheric Research, Wellington, New Zealand

(Manuscript received 15 July 1998, in final form 20 October 1998)

ABSTRACT

Atmospheric blocking events over the South Pacific are investigated using a 39-yr record of 500-hPa height fields from the NCEP–NCAR reanalysis dataset. The analysis extends earlier work using a 16-yr record and confirms that the occurrence of blocking over the southeast Pacific is strongly modulated by the ENSO cycle during austral spring and summer. Comparison of results at 500 hPa with the 300-hPa meridional wind component showed that blocking events are associated with large-scale wave trains lying across the South Pacific from the region of Australia to southern South America. Similar wave trains are evident in both hemispheres in singular value decomposition analyses between 300-hPa meridional wind components and tropical Pacific outgoing longwave radiation (OLR) anomalies.

The hypothesis that the divergence associated with tropical OLR anomalies forces an extratropical wave response that results in enhanced blocking over the southeast Pacific was tested using a linearized, barotropic vorticity equation (BVE) model. Observed 300-hPa mean flow fields and divergence forcing that matched the anomalous OLR were used to drive the BVE model. The resulting pattern of meridional wind and streamfunction anomalies agrees closely with observations. When the tropical OLR anomaly is given an eastward phase speed of 5° per day, the extratropical response agrees even better with observations. This suggests that linear Rossby wave propagation provides an important link between anomalous convection in the Tropics and the occurrence of blocking over the southeast Pacific Ocean.

1. Introduction

The phenomenon of blocking, a breakdown in zonal winds associated with persistent high-latitude ridging, continues to be a major source of error in medium-range forecasts of the global circulation (Tibaldi et al. 1994; Renwick and Wallace 1996a). Difficulty in forecasting blocking events arises because the life cycle of blocking anticyclones is influenced by relatively unpredictable transient baroclinic waves (Shutts 1983; Mullen 1987; Nakamura and Wallace 1993).

While baroclinic wave activity is implicated in blocking, lower-frequency variability also plays an important role, through direct advective forcing, modification of the structure of the mean flow upon which a blocking anticyclone grows, and modulation of the location and intensity of the storm track. Recent work by Nakamura et al. (1997) showed that the relative importance of forcing on different time- and space scales varies with location. High-frequency forcing was found to be very important on average to blocking development over the North Pacific but quasi-stationary Rossby wave activity often plays a dominant role over Europe.

On the interannual timescale, the phase of the El Niño–Southern Oscillation (ENSO) cycle has been related to the frequency of blocking activity over both the North Pacific (Renwick and Wallace 1996b) and the southeast Pacific (Renwick 1998, hereafter R98). Differences in blocking frequency were found to be related to changes in both the mean and the variance of the circulation, in a 16-yr record of analyses from the European Centre for Medium-Range Weather Forecasts (ECMWF). Such results suggest that interannual variability in the frequency of occurrence of blocking is somewhat predictable, although the details of individual events may not be well forecast.

ENSO-related interannual variability in blocking frequency suggests that the occurrence of blocking is related to the propagation of energy from the Tropics. The most likely connection is a Rossby wave response to anomalous tropical heating, as proposed for other locations in the work of Horel and Wallace (1981), Hoskins and Karoly (1981, hereafter HK81), Hoskins and Ambrizzi (1993, hereafter HA93), Rasmusson and Mo (1993), Tyrrell et al. (1996), and Ambrizzi and Hoskins (1997). Here, we explore blocking over the southeast Pacific Ocean and its association with wave propagation from the Tropics. This work extends the data analysis reported in R98 through the use of a 39-yr time series of NCEP analyses, combined with sea surface temper-

Corresponding author address: J.A. Renwick, NIWA Wellington, P.O. Box 14901, Wellington, New Zealand.
E-mail: J.Renwick@niwa.cri.nz

ature (SST) and outgoing longwave radiation (OLR) information. The analysis of observational data leads on to a series of simple barotropic modeling experiments designed to identify whether a linear Rossby wave response to observed tropical diabatic beating anomalies can account for observed midlatitude circulation anomalies.

A description of the datasets and statistical methods used is given in the following section. The observational data analysis is presented in section 3, beginning with basic circulation and blocking statistics and leading to a discussion of observed links between the midlatitude circulation and tropical variability. Section 4 describes several modeling experiments using the observed OLR anomalies to force the linearized barotropic vorticity equation (BVE). A general discussion of results is given in the final section.

2. Data and methods

Analysis of the large-scale circulation in the extratropics is based on a 39-yr time series (1958–96) of 500-hPa geopotential heights (H500) and 300-hPa meridional wind components (V300) from the National Centers for Environmental Prediction–National Center for Atmospheric Research (NCEP–NCAR) reanalysis project (Kalnay et al. 1996). The data were sampled once daily at 1200 UTC at 2.5° latitude–longitude resolution. The H500 fields were projected onto a relatively coarse 361-point Southern Hemisphere polar stereographic grid, which covers all latitudes south of 20°S, as used in R98. The raw H500 anomalies were temporally filtered to obtain 6-day and 30-day low-pass (LP) filtered data, using 51-point moving average filters with half-power points at 6 and 30 days. The 30-day low-pass filter is the same as that used in R98.

A 17-yr (1980–96) record of pentad-mean OLR obtained from NCEP (Kayano et al. 1995) was used as a proxy for convective activity and diabatic heating in the Tropics. Data were selected at all longitudes between 45°S and 20°N on a 5° latitude × 10° longitude grid, from the original global 2.5° resolution grid. ENSO-related variability was represented in terms of monthly mean sea surface temperature information taken from the United Kingdom Meteorological Office Hadley Centre ''GISST 2.3A'' dataset (Parker et al. 1994) on a 5° × 5° latitude–longitude grid between 60°S and 20°N, over the same 39-yr period as used for the NCEP reanalyses.

Climatologies were calculated for the H500, V300, and OLR data series as the first two harmonics of the daily (or pentad) time mean at each grid point. For the SST data, the climatology was defined as the time mean for each month at each grid point. All datasets were converted to anomalies by subtraction of their respective climatologies.

Spurious trends may be present in the NCEP–NCAR reanalyses. These could arise from gradual changes in the observing network over the 39-yr span of the analyses and possibly from the inclusion of incorrectly located Australian Bureau of Meteorology ''PAOB'' data in the period 1979 through 1992 (described in http://wesley.wwb.noaa.gov/paobs/paobs.html). Analysis of Southern Hemisphere low-frequency variability in the reanalyses (Kidson 1999) has shown up an apparent discontinuity in upper-tropospheric circulation statistics around 1970.

The H500 data were therefore analyzed for inhomogeneities and trends before any further processing of reanalysis fields. A long-term linear trend was fitted at each grid point and variances were calculated in a number of frequency bands, in three 13-yr periods. Covariance-based empirical orthogonal functions (EOFs; Jolliffe 1986) and Varimax-rotated EOFs (REOFs) were also calculated for each period and frequency band, and compared for consistency between periods. Brief results are presented in the following section.

Following the above preprocessing, we extended the blocking study of R98 using the longer NCEP–NCAR H500 dataset. As in R98, blocking events were identified as persistent positive projections upon a pair of spatial patterns, centered over the southeast and southwest Pacific. Such an approach is analogous to that used by Renwick and Wallace (1996b) for the North Pacific and produces results similar in many respects to the analysis of ''persistent positive anomalies'' by Dole (1986).

Blocking signatures identified in H500 data were compared to V300 fields through compositing and correlation analyses in an effort to identify blocking-related wave propagation. Linkages between the midlatitude circulation and tropical variability were then assessed through singular value decomposition analysis (SVDA; Bretherton et al. 1992; Renwick and Wallace 1995) of pairs of datasets (OLR and V300, OLR and H500, etc). To investigate physical mechanisms responsible for observed REOF and SVDA results, a number of BVE model simulations were carried out. The model was forced with divergence anomalies calculated from observed OLR anomaly patterns, using observed background mean flows. Keeping the shape of the forcing constant, the sensitivity of the response to the location of the forcing and to the mean state was investigated.

3. Observational results

a. Homogeneity of H500 fields

The raw daily H500 anomalies were first analyzed by detection of linear trends, as discussed above. Highly significant (99% significance level, or higher) temporal trends were found at most grid points. Figure 1 shows the mean trend, in geopotential meters per decade. Shading indicates areas where trends were not significant. The basic pattern shows a strengthening of the polar vortex and an increase in mean zonal winds between

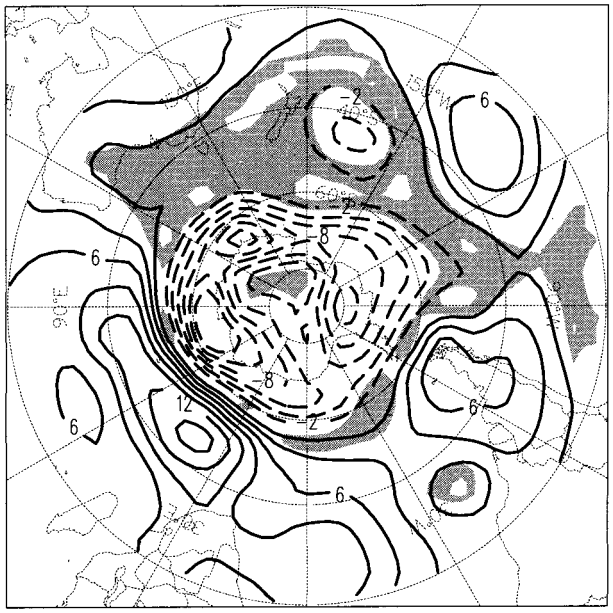

FIG. 1. Linear temporal trend in NCEP–NCAR H500 field. Units are m decade^{-1}. The contour interval is 2, negative contours are dashed, and the zero contour has been omitted. Shading indicates regions where the trend is not significant at the 99% level.

50° and 60°S, especially over the Indian Ocean. In the region of southeast Pacific blocking investigated in R98, the trend has been for a small mean height decrease. The pattern illustrated in Fig. 1 may be related to changes in the observational data network over the years and/or may indicate genuine decadal-scale variability in the circulation.

The mean trend was removed at each grid point for H500, and for V300, where significant trends were concentrated in the tropical Pacific and near the Antarctic coast. After removal of the linear trend and the mean seasonal cycle (described above), the variance of the H500 fields was examined for the three consecutive 13-yr periods within the 39-yr record. Variance fields were very nearly identical in all periods, for the raw anomalies and for 6-day high-pass (HP) and 30-day LP filtered data. The three leading REOFs in each frequency band appeared to be relatively stable in time, especially at low frequency where spatial correlations between matching modes in different 13-yr periods all exceeded 0.7. The leading three REOFs of the raw anomalies and the leading two of the 6-day HP filtered anomalies exhibited spatial correlations exceeding 0.6 between all pairs of samples. All rotations were based on the leading 12 EOFs in each case. On the basis of the above analysis, the NCEP reanalysis data were taken to be ''homogeneous,'' after removal of linear trends.

b. Basic circulation and blocking statistics

The variance and REOF structure of the reanalysis H500 anomaly field is very similar in form to that found in R98, using a shorter record of ECMWF data. The standard deviation of the 30-day LP anomalies is plotted in Fig. 2, along with the standard deviation of the seasonal and annual mean anomalies. The variance maximum over the southeast (SE) Pacific becomes more prominent as the averaging period increases, up to at least the interannual timescale.

The three leading REOFs of the 30-day LP anomalies were almost identical in form to those presented in R98 (spatial correlations >0.95), as shown in Fig. 3. As in R98, the form of the leading REOFs was very stable over a wide range of rotation dimensions. A rotation using 12 EOF dimensions was used for all further analysis, for consistency with R98. Following the methodology of R98, the raw H500 anomalies were projected upon 30-day LP REOFs 2 and 3 to produce daily ''blocking index'' amplitude time series for the SE and southwest (SW) Pacific, respectively. Below, we concentrate on SE Pacific blocking.

Blocking events were identified from the blocking index amplitude time series. Cases where the amplitude was at least 0.5 standard deviations above average for at least 5 days were counted as ''blocks.'' Much of the analysis described below was repeated with an amplitude threshold of 1.0 standard deviations. Results were very similar in form, apart from an approximate 50% decrease in the number of blocking cases identified. Blocking occurrences were summed over each season and annually. Basic occurrence and duration statistics (Table 1) agreed very well with ECMWF-based results shown in Table 1 of R98.

Interannual variability in blocking frequency also agreed well with that found using ECMWF data, for the period 1980–95 (temporal correlations were $\sim$0.9 in all seasons). Variability in blocking frequency over the SE Pacific is illustrated in Fig. 4. The apparent temporal trend in SE Pacific blocking frequency over the ECMWF data period is less dramatic in the reanalyses. Data for the full 39-yr period do not show significant linear trends in any season.

Blocking occurrence was stratified by the phase of the ENSO cycle, as in R98. The occurrence of El Niño ''warm'' events was defined objectively from a combination of Southern Oscillation index (SOI) and ''NINO3'' SST values (as suggested in Trenberth 1997). An El Niño event was defined to occur when the 6-month mean SOI was less than -0.8 or the NINO3 SST anomaly was greater than $+0.8$ K. Using these criteria, warm El Niño conditions were deemed to occur during the Austral spring/summer (September–February, SONDJF) beginning in September of 1963, 1965, 1969, 1972, 1976, 1977, 1982, 1986, 1987, 1991, 1992, and 1994. All other years are taken together and are denoted ''non–El Niño'' years.

Tables 2 and 3 shows differences in South Pacific blocking frequency, stratified by the phase of ENSO, for the 39-yr reanalysis period. The significant ENSO-related modulation of SE Pacific blocking reported in

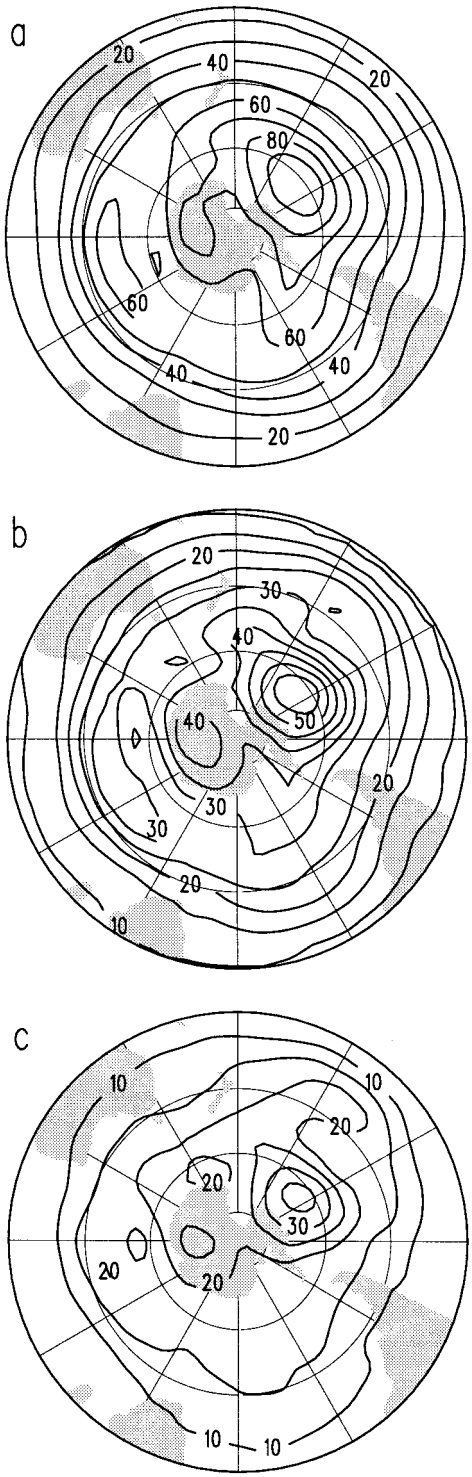

FIG. 2. H500 standard deviations (m) for (a) 30-day low-pass filtered, (b) 3-month mean, and (c) 12 month mean data. The contour interval in (a) is 10 m and is 5 m in (b) and (c).

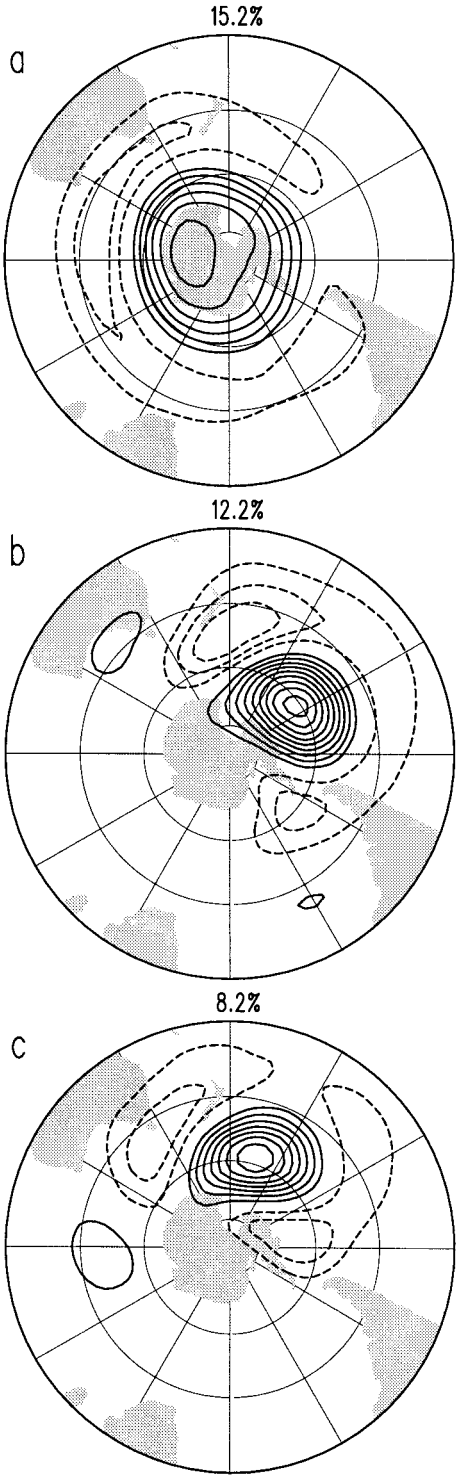

FIG. 3. The three leading REOFs of 30-day low-pass filtered H500 fields, shown as covariance maps. The contour interval is 10 m, negative contours are dashed, and the zero contour has been omitted. Figures at the top of each panel indicate the fraction of low-pass filtered variance accounted for by each REOF.

TABLE 1. Statistics of blocking events defined by persistent positive projections upon REOFs 2 and 3 of 30-day low-pass filtered 500-hPa height anomalies (Fig. 3). All events between 1958 and 1996 are included. Intensity and duration thresholds are +0.5 standard deviations and 5 days, respectively. Duration figures are in days.

	SE Pacific	SW Pacific
REOF center of action	59°S, 124°W	54°S, 166°W
Number of events	328	357
Total number of days	3560	3515
Median, max duration	8, 46	8, 40

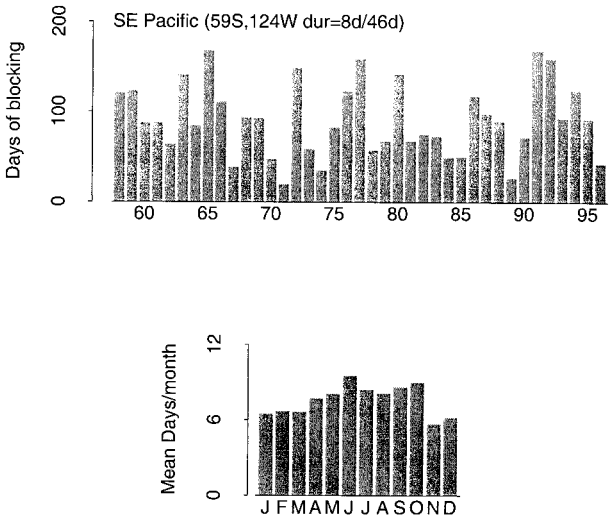

FIG. 4. Interannual and seasonal variability in SE Pacific blocking frequency, as the number of days of blocking per calendar year (top) and the mean number of days per month (bottom). The caption on the top panel indicates the location of the center of the relevant REOF pattern and the median and maximum block duration (days).

R98 is clearly evident in the reanalysis data. Warm events in the Tropics are associated with enhanced SE Pacific blocking frequency in all seasons, especially during austral spring (SON). Approximately twice as many days of blocking occur over the SE Pacific in SONDJF during the warm phase of ENSO than during the normal or cool phase.

The effect of ENSO upon blocking frequency is less systematic over the SW Pacific. Mean differences change sign from one season to the next, with no net effect averaged over the year as a whole. ENSO-related differences were statistically significant in winter (June–July–August, JJA) where El Niño events are on average associated with a decrease in blocking frequency. There is a strong but nonsignificant relationship in the opposite sense in the following three months.

The strength of the ENSO signal may also be estimated by correlating the averaged blocking index with the SOI. Over the whole 39 years, the correlation coefficients during SON and SONDJF are around −0.6. Using a relatively short time window (e.g., 15 yr) to move through the time series, the strength of the blocking/SOI correlation increases over time in summer (DJF) and decreases in winter (JJA). The SONDJF correlation is around −0.6 through to the early 1980s and then decreases to near −0.8 by the end of the record (the most recent 15 yr). Such an effect may reflect the preponderance of El Niño events over the last 20 years, or may reflect decadal-scale changes in the strength of ENSO events and their teleconnections.

ENSO-related variations in the Southern Hemisphere (SH) extratropical circulation during SONDJF are summarized in Fig. 5 in terms of mean warm/cool year height differences and variance ratios for unfiltered height anomalies. The mean pattern is very similar to that found in R98, but the region of significant high-latitude variance increase is displaced south and east compared to the ECMWF-based result. The mean height difference pattern is very similar in form to ENSO-related EOF patterns found on interannual and intradecadal timescales by Kidson (1999) and Kiladis and Mo (1998).

c. Wave propagation and blocking

A series of compositing and correlation studies were carried out to identify the characteristics of upper-tropospheric wave activity associated with blocking events. The upper-tropospheric flow over the Pacific was characterized in terms of the meridional component of the unfiltered daily 300-hPa wind anomalies (V300).

Figure 6 shows mean meridional wind patterns before, during, and after the 159 SE Pacific blocking events occurring between September and February, identified from 500-hPa height anomaly time series as described above. Lag correlation maps between V300 and the southeast Pacific blocking index during SONDJF are shown in Fig. 7. In both figures, a wave

TABLE 2. Interannual variability in days of blocking over the southeast Pacific, 1958–96. Years are stratified by the phase of ENSO. The first two lines show the mean and interannual standard deviation of the number of days of blocking in each of the periods indicated. The *t* value for the warm–cool difference in means is shown along with the percent probability that the mean difference is zero. The bottom line indicates the percentage of all possible mean subsample differences exceeding the observed ENSO-related difference. Statistics suggesting at least 95% significance are indicated in boldface.

	Annual	MAMJJA	SONDJF	MAM	JJA	SON	DJF
El Niño	124 ± 36	60 ± 21	64 ± 21	28 ± 13	31 ± 16	37 ± 17	26 ± 13
Non–El Niño	79 ± 34	45 ± 25	34 ± 19	21 ± 16	24 ± 16	17 ± 14	17 ± 14
t statistics	**3.4, 0.3**	1.8, 9.4	**4.0, <0.1**	1.3, 20	1.3, 22	**3.6, 0.2**	1.8, 8.2
Percent exceeding	**0**	6	**0**	11	10	**0**	**4**

TABLE 3. As in Table 2 but over the southwest Pacific.

	Annual	MAMJJA	SONDJF	MAM	JJA	SON	DJF
El Niño	90 ± 24	47 ± 20	44 ± 15	32 ± 21	15 ± 7	24 ± 12	20 ± 9
Non–El Niño	90 ± 28	53 ± 19	36 ± 17	29 ±13	24 ± 14	15 ± 13	22 ± 13
t statistics	−0.1, 0.3	−0.7, 48	1.3, 19	0.5, 34	**−2.6, 1.5**	2.0, 5.3	−0.6, 48
Percent exceeding	50	22	11	28	**2**	**2**	28

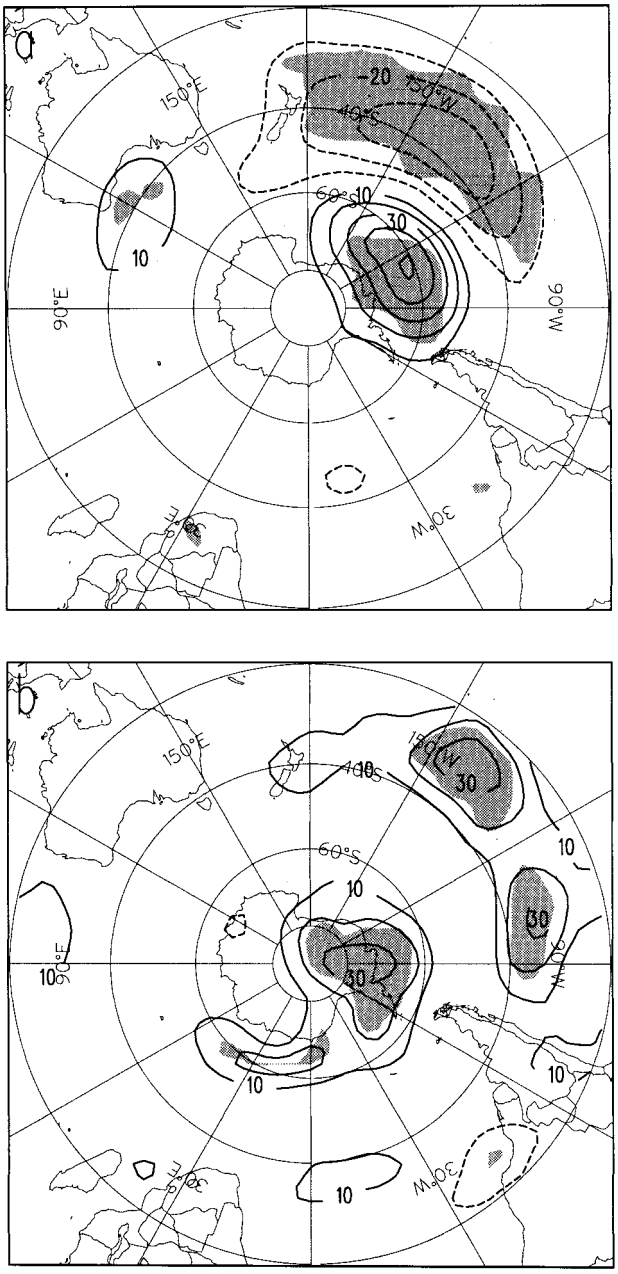

FIG. 5. ENSO-stratified differences in (a) the mean and (b) the variance of unfiltered H500 fields during SONDJF. (a) The mean taken over El Niño years minus the mean taken over all other years (contour interval 10 m). (b) The ratio of variances between El Niño years and all other years, expressed as a percentage difference from 100% (contour interval 10%). In both cases, negative contours are dashed, the zero contour has been omitted and shading indicates 99% significance.

train is evident before, during, and after the blocking event. The horizontal scale equates to zonal wavenumber 4 throughout, but wave amplitude becomes concentrated over the South Pacific during the blocking event itself. The composite and correlation patterns exhibit a similar structure in all seasons, but exhibit maximum amplitude during austral winter and spring.

The waves appear to originate over Australia, curving south over the central Pacific toward the southern tip of South America, like the meridional wave train identified by Karoly et al. (1989) using the stationary wave flux vector of Plumb (1985). The poleward and eastward arching of this pattern is characteristic of remotely generated Rossby waves, possibly forced in tropical regions, as illustrated for example in Jin and Hoskins (1995, hereafter JH95). There is evidence in the maps of phase propagation of around 5° longitude per day (~6 m s^{-1} at the equator).

The link between tropical forcing and extratropical wave propagation was explored observationally through SVDA between OLR anomalies over the tropical Pacific and the extratopical circulation represented as pentad-mean V300 anomalies. The most spatially coherent response was obtained with OLR leading V300 by two pentads (10 days). The leading mode of a two-pentad lag SVDA between pentad-mean OLR and pentad-mean V300 during SONDJF is shown in Fig. 8, as a pair of covariance maps. The amplitude time series of the two modes have a correlation of 0.49. Standard significance tests (Craddock and Flood 1969; North et al. 1982) applied to the squares of the singular values (Bretherton et al. 1992) suggest that the leading SVDA mode is well separated from subsequent pattern pairs.

The OLR pattern shows an east–west dipole with suppressed convection (enhanced OLR) over the Maritime Continent and enhanced convection (decreased OLR) centered near the date line. This mode is closely associated with ENSO on the interannual timescale (Rasmusson and Mo 1993) and is very similar in form to the leading EOF of the OLR field. The V300 pattern shows wave trains in both hemispheres having the largest amplitude in the Northern Hemisphere, over the Gulf of Alaska where the variance of the V300 field is a maximum. In the SH, a wave train lies from Australia, across the South Pacific, to southern South America. The leading V300 mode is very similar in form but has larger amplitude if the domain of the V300 field is restricted to the SH (not shown). It is similar in form to the ''blocking midpoint'' V300 composite (Fig. 6) and

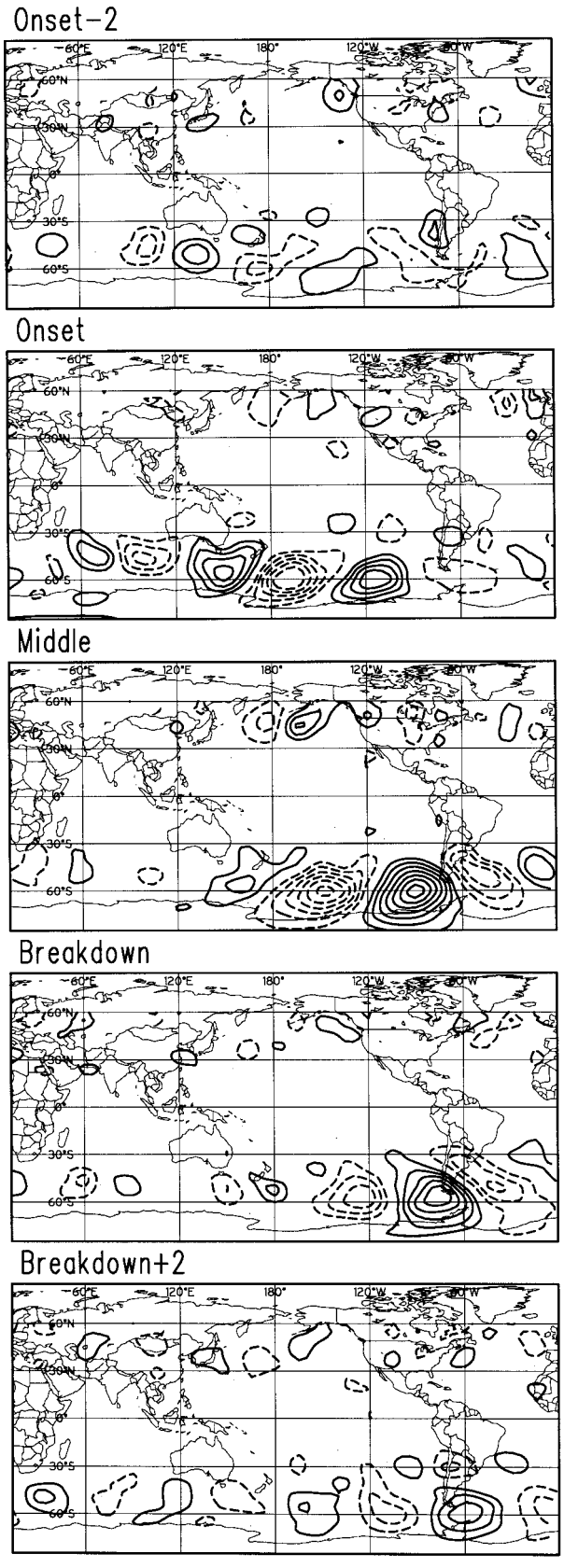

the contemporary correlation map between V300 and the southeast Pacific blocking index (Fig. 7).

Analysis of other pairs of time series (not shown) produced results consistent with those discussed above. SVDA between OLR and pentad-mean H500 produced a very similar leading OLR pattern associated with a strong positive height anomaly over the SE Pacific. Monthly mean Pacific SST paired with monthly mean V300 or H500 revealed a leading mode consisting of an ENSO-like SST pattern concentrated along the equator, again associated with positive height anomalies and an upper-level wave train across the South Pacific, but somewhat ''smeared out'' zonally due to the time averaging.

The above data analysis has established a statistical connection between anomalous tropical convection and extratropical Rossby wave propagation. We now use a linearized BVE model to explore dynamical links between these events.

4. Modeling experiments

In this section, we describe a series of simple barotropic modeling experiments that were performed to identify whether a linear Rossby wave response to observed tropical diabatic heating anomalies could account for observed midlatitude circulation anomalies. Tropical OLR anomalies at the top of the atmosphere are taken to be the mean signature of tropical convection and an associated vertical motion field. Since the vertical motion can be assumed to be zero at the top of the atmosphere, by continuity at upper levels there must be corresponding divergence (convergence) above upward (downward) motion at middle levels. Thus we interpret the tropical OLR anomaly field (Fig. 8), identified by the SVDA, directly as a divergence anomaly and use it to force a barotropic model, linearized about a range of mean flows.

a. The model

The barotropic model used to calculate the far-field response to divergence forcing follows that of HA93. The model equation can be written as

$$\frac{\partial \xi}{\partial t} = F, \tag{1}$$

where

$$F = -\nabla \cdot [\mathbf{v}(\zeta + fh/H)] + \lambda(\xi_0 - \xi) + \mu\nabla^6\xi. \tag{2}$$

←

FIG. 6. V300 composites, relative to timing of SE Pacific blocking events during SONDJF. Composites are taken over 159 cases, from 2 days before block onset (top) through 2 days after breakdown (bottom). ''Middle'' indicates the middle day of the blocking event. The contour interval is 2 m s^{-1}, negative contours are dashed, and the zero contour has been omitted.

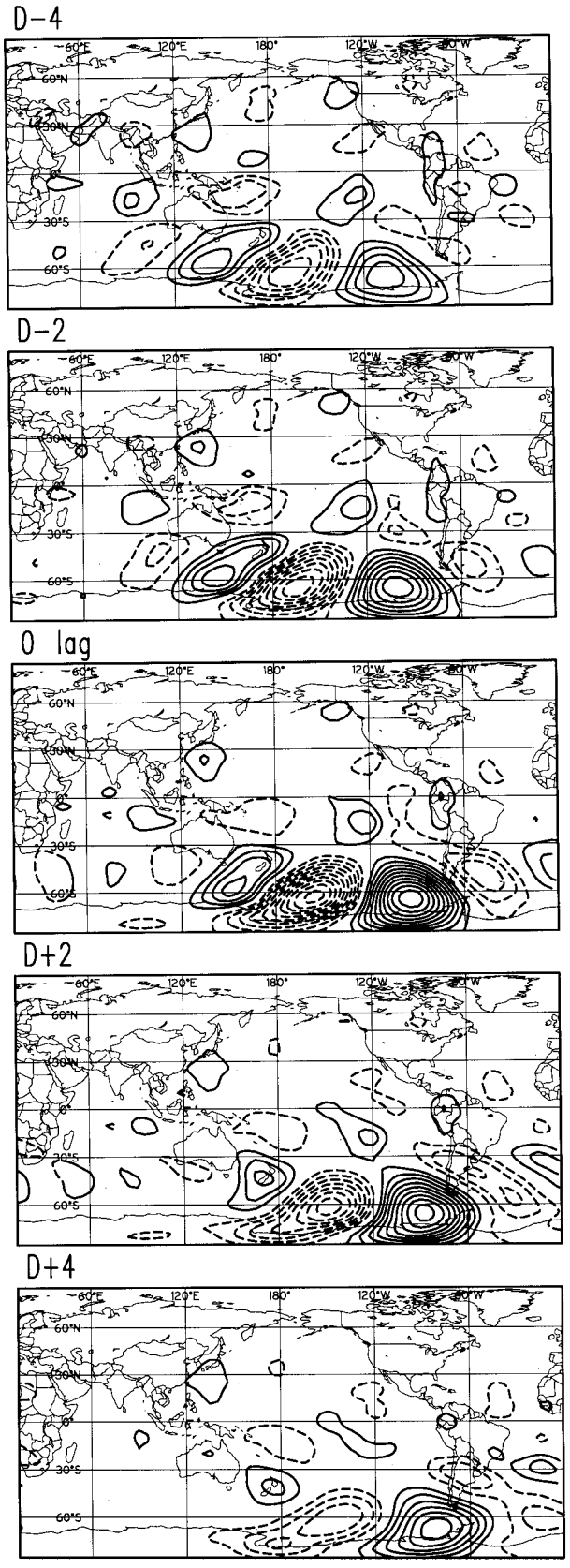

In (2), ξ is the relative vorticity, f is the Coriolis parameter, h is the orographic height, H is the pressure scale height, ζ is the absolute vorticity ($\xi + f$), and $\mathbf{v}$ is the wind vector with $\mathbf{v}_\psi$, $\mathbf{v}_\chi$ the rotational and divergent components. In addition, μ determines the timescale over which the shortest length scale is dissipated and λ determines the timescale over which ξ is relaxed back to the mean ξ_0.

The orographic height h was set to zero. Separating the wind $\mathbf{v}$ into its rotational and divergent components $\mathbf{v}_\psi$, $\mathbf{v}_\chi$ we can write F above as

$$F = -\mathbf{v}_\psi \cdot \nabla\zeta - \nabla \cdot (\mathbf{v}_\chi \xi) + \lambda(\xi_0 - \xi) + \mu\nabla^6\xi. \quad (3)$$

Linearizing (1) about a climatological mean state, denoted by an overbar with anomalies denoted by primes, we get

$$\frac{\partial \xi'}{\partial t} + \bar{\mathbf{v}}_\psi \cdot \nabla\xi' + \mathbf{v}'_\psi \cdot \nabla\bar{\zeta} = -\nabla \cdot (\mathbf{v}'_\chi \bar{\zeta}) - \overline{\nabla \cdot (\bar{\mathbf{v}}_\chi \xi')} - \lambda\xi' + \mu\nabla^6\xi'. \quad (4)$$

The perturbation vorticity was typically an order of magnitude smaller than the mean vorticity, while the mean divergent wind was of a similar magnitude to the perturbation divergent wind corresponding to the OLR forcing. Thus, the second (overbarred) source term on the right-hand side (rhs) of (4) was neglected, giving as our linearized, damped, barotropic vorticity equation

$$\frac{\partial \xi'}{\partial t} + \bar{\mathbf{v}}_\psi \cdot \nabla\xi' + \mathbf{v}'_\psi \cdot \nabla\bar{\zeta} = -\nabla \cdot (\mathbf{v}'_\chi \bar{\zeta}) - \lambda\xi' + \mu\nabla^6\xi'. \quad (5)$$

Assuming the mean state ξ_0 is being maintained by other processes (e.g., baroclinic and orographic), here represented by the linearization and dissipation terms, running the model for about 10 days (the time taken for the tendency term to become small) gives the linear stationary Rossby wave response ξ' to tropical forcing by the imposed divergent wind field $\mathbf{v}'_x$. Equation (5) was solved by the spectral transform technique, with a triangular truncation at wavenumber 42. This corresponds closely to the 2.5° resolution of the data used for the background mean wind fields and tropical OLR forcing. In the following experiments, μ was chosen to give a 6-h e-folding time for dissipating the two-grid interval wave and λ chosen to restore the vorticity to its initial value with an e-folding time of 10 days. The spatial phase of the wave responses was found not to

←

FIG. 7. Maps of correlation between V300 and SE Pacific blocking index during SONDJF, at lags up to 4 days. D-4 and D-2 indicate that the blocking index leads by 4 and 2 days, respectively. The central panel is the contemporary correlation and the blocking index lags in the bottom two panels. The contour interval is 0.05, negative contours are dashed, and the zero contour has been omitted.

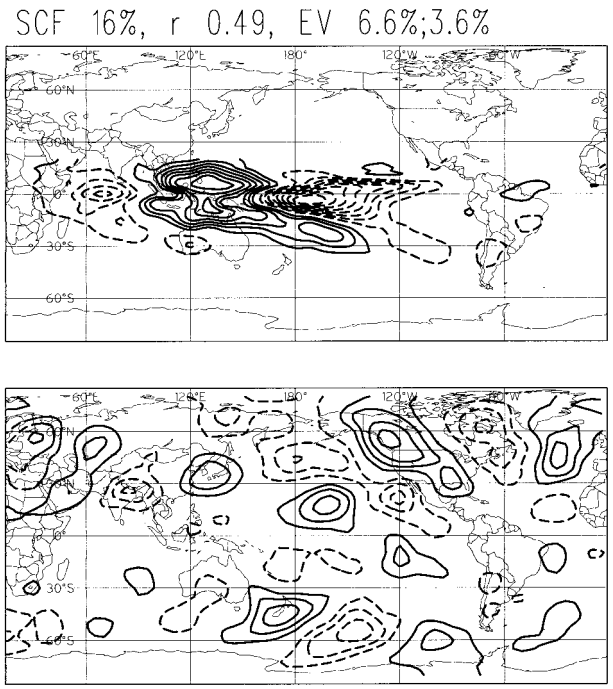

FIG. 8. Covariance maps (OLR homogeneous, V300 heterogeneous) representing the first mode of a two-pentad (10 day) lagged SVDA between pentad-mean OLR anomalies over the tropical Pacific Ocean and V300 over the globe, two pentads later, during SONDJF. The contour interval in the top panel (OLR) is 2.5 W m^{-2} and is 0.5 m s^{-1} in the bottom panel (V300). In both panels, negative contours are dashed and the zero contour has been omitted. Statistics printed are the squared covariance fraction, temporal correlation between the expansion coefficient time series, and respective explained variance.

be sensitive to the precise values of these constants, as has also been reported by Hoerling et al. (1997).

For a range of climatological initial states, (5) was forced by the divergent wind field shown as streamlines and isotachs in Fig. 9. The forcing consisted of divergence in the middle to eastern tropical Pacific with convergence over the Indonesian region—an anomalous Walker circulation with spatial pattern exactly matching the OLR anomaly shown in Fig. 8. The OLR pattern may vary between different El Niño years, but the data analysis of section 3 indicates that on average this pattern dominates the OLR signal when blocking is strong in the South Pacific. Considering the response to tropical heating in a baroclinic atmosphere, JH95 have demonstrated with a multilevel spectral model that the 300-hPa level is the most relevant for single-level studies. Therefore, the barotropic model was run for a range of initial states consisting of rotational wind fields at 300 hPa averaged over the 39 years of the NCEP reanalysis dataset.

b. Results

1) SEPTEMBER TO FEBRUARY MEAN FLOW

We chose the period SONDJF for our first experiment as it was during this time that the observed blocking teleconnection pattern was strongest. The corresponding mean flow is shown as streamlines and isotachs in Fig. 10. Note the region of easterlies within 10° of the equator, and the main jets at 45° in both hemispheres plus the Australasian jet at about 28°S. The Rossby wave response is displayed in Fig. 11 as wind vectors plus shading and isotachs of the v component of the wind. The modeled wind field response in the SH matches the observed wind anomaly in Figs. 5 and 6 fairly well, clearly showing the Rossby wave response arching south and east from a source just west of Australia to give the correct phase in the southeast Pacific. The horizontal scale is somewhat too large, being close to zonal wavenumber 2 or 3 rather than 3 or 4 as observed, although this does vary with longitude. The magnitude of the response of some 6 m s^{-1} is realistic, requiring a divergence in the Tropics of about 3×10^{-6} s^{-1}, which, according to Ambrizzi and Hoskins (1997), implies a

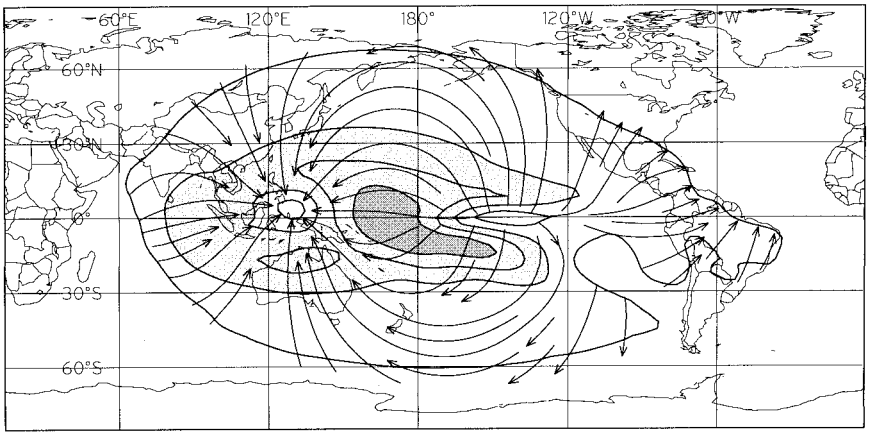

FIG. 9. Streamlines and isotachs for the forced divergent wind field matching the OLR anomaly pattern in Fig. 8. Contours are every 0.5 m s^{-1} with shading changes at 1 and 2 m s^{-1}.

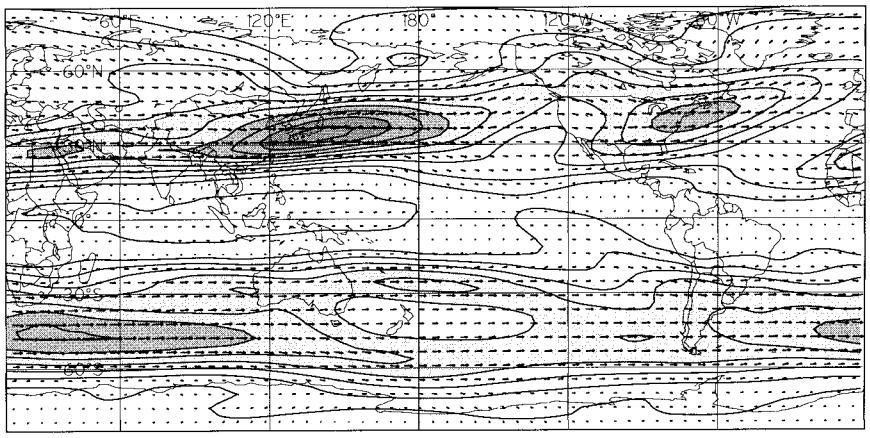

FIG. 10. Full wind vectors and isotachs for the NCEP 40-yr mean Sep–Feb 300-hPa flow. Contours are every 5.0 m s^{-1} with shading changes at 20, 30, and 40 m s^{-1}.

rain rate of 5 mm day^{-1}. In the model runs the forcing divergence was actually scaled down by a factor of 30 to keep the calculations linear, but the resulting fields scaled back up for presentation.

Although the main divergence and convergence regions associated with the forcing are near the equator at 150°W and 120°E, respectively (Fig. 9), the source of Rossby waves appears to be just west of Australia, at about the latitude of the subtropical jet. This can be explained by considering the first term on the rhs of (5), called the Rossby wave source (RWS) term by Sardeshmukh and Hoskins (1988, hereafter SH88). The RWS term can be expanded to

$$\text{RWS} = -\nabla \cdot (\mathbf{v}_x'\overline{\zeta}) = -\overline{\zeta}\nabla \cdot \mathbf{v}_x' - \mathbf{v}_x' \cdot \nabla\overline{\zeta} \qquad (6)$$

and is shown in Fig. 12 for the SONDJF mean flow and OLR anomaly forcing in Fig. 9.

The divergence/convergence contribution [the first RWS term in (6)] appears as a pair of dipoles near the equator, within the equatorial easterlies, as can be seen from Fig. 10. However, SH88 emphasized the importance of the second RWS term, particularly when specifying divergence in regions of equatorial easterlies, as is the case here. Following the wave dispersion and ray tracing ideas outlined in HK81, and summarized in HA93, Rossby waves propagate only in regions of westerlies, while in easterlies they are evanescent. The contribution from the second RWS term can be seen at about 120°E concentrated near the latitudes of the major jet streams. Its major contribution comes from the product of the v component of the forced divergent wind and the poleward gradient of mean absolute vorticity β_*. Sometimes, β_* is known as the effective beta parameter $\beta - U_{yy}$, and the Mercator coordinate equivalent (β_M of HK81) for the SONDJF mean flow is shown in Fig. 13. The contribution of the U_{yy} term is clearly evident in the region of the major jet streams. HK81 have also shown that the wavenumber K_S associated with the sta-

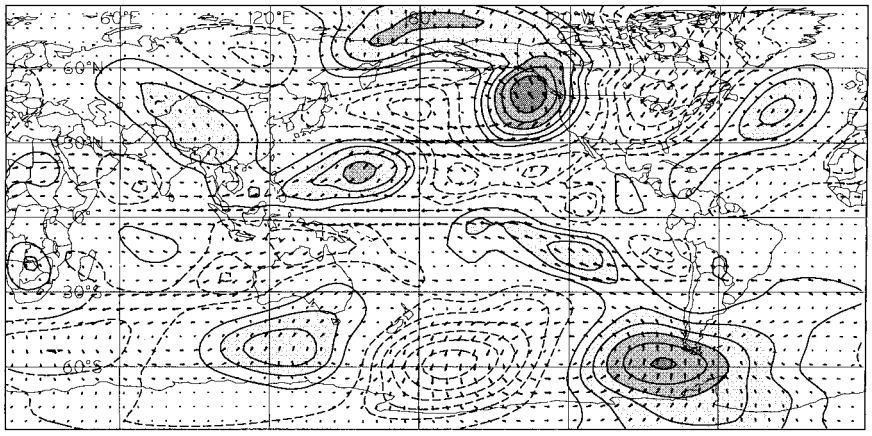

FIG. 11. Rotational wind vectors plus shading and isotachs of the v component of the wind for the linear, barotropic, Rossby wave response after 10 days to the forcing in Fig. 9 for the basic flow in Fig. 10. Contours are every m s^{-1} with shading changes at 2 and 4 m s^{-1} and the zero contour has been omitted.

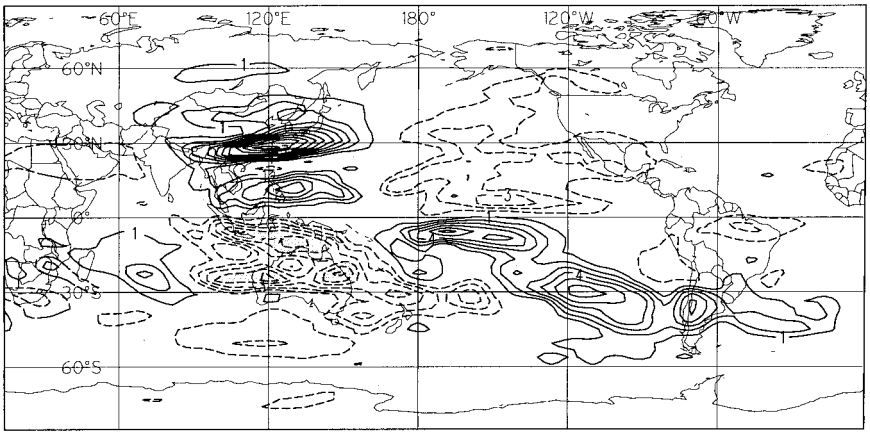

FIG. 12. Rossby wave source term for the forcing in Fig. 9 and the basic flow in Fig. 10. Units are $\Omega^2\ s^{-2}$ where Ω is the earth's rotation rate in radians per second. Contours are every $\Omega^2\ s^{-2}$ with shading changes at values of -4 and -6.

tionary wave response is $(\beta_M/u_M)^{1/2}$. This is shown in Fig. 14 for the SONDJF mean flow. Evanescent regions in the Tropics and on the poleward side of the major jet streams can be seen. In general K_S decreases from values of about 8 at 20° latitude, to values of 2 or 3 at 55° latitude. As can be seen in Fig. 11, wavenumbers 2 to 3 dominate the response in the southeast Pacific, in approximate agreement with simple ray tracing arguments and observations.

2) SENSITIVITY TO MEAN FLOW

For the same OLR/divergence forcing we also considered the response using the *zonally averaged* SONDJF mean flow (Fig. 15). In the SH, the amplitude was decreased slightly and now followed the more northerly path of the mean flow maximum, but the phase and shape was affected very little. As explained in HA93 the jets tend to act as waveguides. In the NH the response was much more like a mirror image of that in the SH, since the strong Asian and North American jets were now diminished and spread out, leading to a weaker, lower-wavenumber response over North America.

We repeated the above experiments for the middle months of each of the four seasons (not shown) and found changes in the responses could be explained by the waveguide and ray tracing theory contained in HA93 and HK81. In particular, for July the response in the SE Pacific was dominated by waves 1 and 2 and displaced some 30° eastward. The variation between the winter and summer responses was markedly different between the hemispheres. In the Southern Hemisphere there was a moderate response all year round, whereas for the Northern Hemisphere the response was large in January and April, but almost disappeared during July and October.

3) VARYING THE FORCING LONGITUDE

In order to further test the robustness of the Rossby wave response, we moved the location of the OLR forcing $\pm 30°$ longitude relative to that shown in Fig. 9. To a first approximation the responses (not shown) were moved by a matching 30° longitude. In the SH there was some loss of amplitude for the displaced forcing, and for the eastward displacement there was a tendency for the wave response to split about the region just east of New Zealand where K_S goes to zero, with a higher wavenumber response to the north. In the NH there was much greater variation in the response. For the eastward displaced forcing the wave train across the northeast Pacific was amplified. However, for the westward displacement the response was significantly reduced, since the evanescent region to the north and east of the NH jet now interfered with the wave response.

4) ALLOWING THE FORCING TO PROPAGATE

Finally we started the integration with the tropical OLR anomaly initially 60° west of its position in Fig. 9, and allowed it to propagate longitudinally with an eastward phase speed of 5° per day. As the integration progressed a wave response was set up that maximized in the Southern Hemisphere on day 12, shown in Fig. 16, when the OLR forcing had reached the control position. The amplitude of this response, compared to that with the fixed forcing, was slightly diminished as the pattern had been given less time to become established. However, its phase structure was in better agreement with the observations as it now propagated with the observed phase speed of 5° per day and had a slightly shorter wavelength with wave 3 or 4 dominating. This change in structure follows the ray tracing theory of HK81, but applied to a traveling wave. As explained by Karoly (1983), the flow speed u_M in the stationary

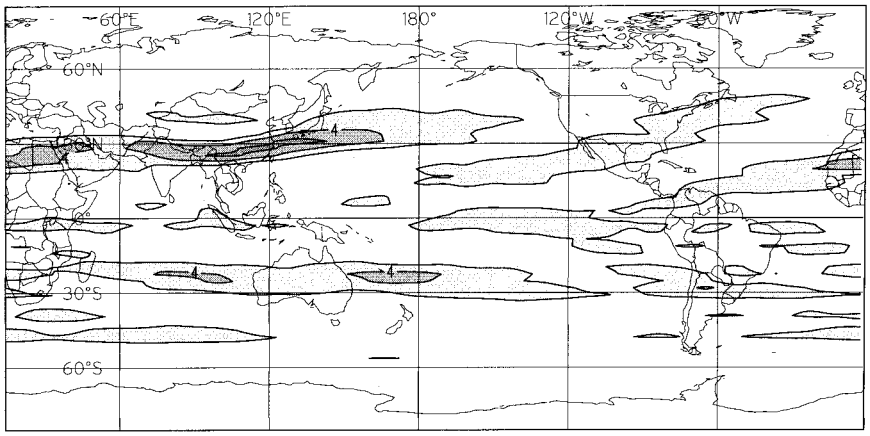

FIG. 13. The Mercator coordinate equivalent (β_M of HK81) of the poleward gradient of mean absolute vorticity for the Sep–Feb mean flow shown in Fig. 10. Units are (Ω/a) m^{-1} s^{-1} where a is the earth's radius. Contours and shading change every two units.

total wavenumber $K_S = (\beta_M/u_M)^{1/2}$, associated with the stationary wave response, is now replaced by the difference between the flow speed and the phase speed $u_M - \omega/k$ in the low-frequency total wavenumber $K_\omega = [\beta_M/(u_M - \omega/k)]^{1/2}$. For an eastward-propagating wave, the nonpropagating region for Rossby waves now extends into the westerlies. Also, rays for higher wavenumbers (4 and 5) now recurve more slowly toward the Tropics, allowing energy associated with them to propagate farther poleward.

The wave response in the Northern Hemisphere (NH) shown in Fig. 16 appears to be worse for the propagating tropical source. However, the NH response on day 18 (6 days later) is in good agreement with the observations. Six days corresponds to 30°, so an explanation for the time difference in the response in the two hemispheres is largely given in section 4b(3) above.

The reason that the Rossby wave response for the BVE maximizes where it does appears to be partly associated with the background flow. The effective beta parameter β_M for the SONDJF mean flow shown in Fig. 12 has a local maximum just west of Australia. As the propagating v component of the forced divergent wind enters this region, the RWS term maximizes. As the tropical forcing continues eastward the Rossby waves then generated over Australia will be interfered with by the region of low K_ω, which begins just west of New Zealand.

c. Summary

For forcing with the form of the tropical OLR anomaly shown in Fig. 9 to create a significant Rossby wave source, it appears the v component of the forced divergent wind must intersect the major jets where the effective beta parameter $\beta - U_{yy}$ takes significant values. To get a significant far-field Rossby wave response to this source, the resulting ray paths must avoid the

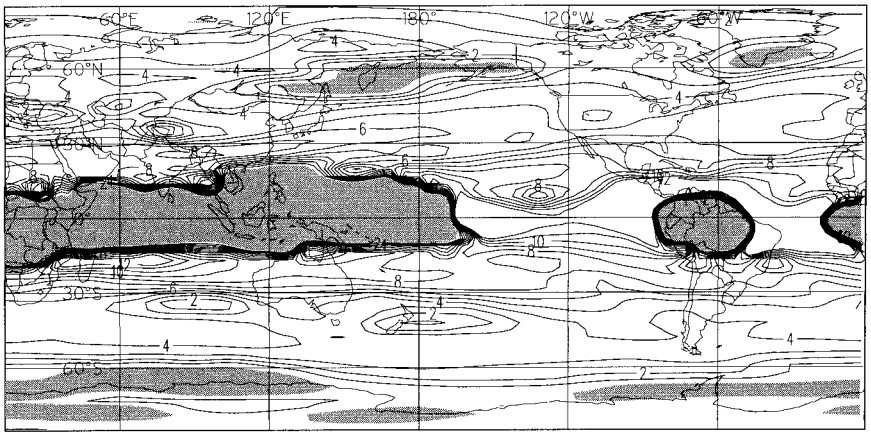

FIG. 14. The total wavenumber $K_S = (\beta_M/u_M)^{1/2}$ associated with the stationary wave response for the Sep–Feb mean flow shown in Fig. 10. Units are $(1/a)$ m^{-1}. Contours every unit up to wavenumber 12. Shading denotes nonpropagating regions.

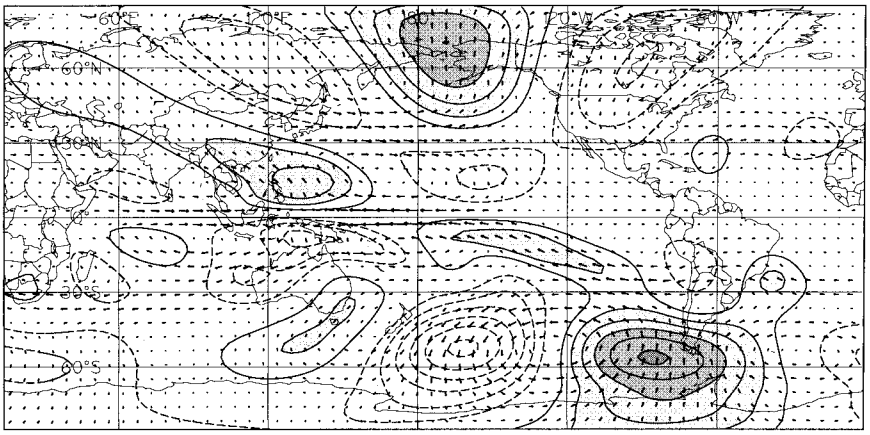

FIG. 15. As in Fig. 11 except for the zonally averaged Sep–Feb mean flow.

evanescent regions where K_s goes to zero (typically in the tropical easterlies and just poleward of the major jets). These requirements appear to be met here for the above propagating OLR anomaly and mean flow during the SH spring/summer. Thus, the ray tracing theory of HK81 applies and the observed ''blocking'' in the southeast Pacific can be at least partly explained as the linear Rossby wave response to a traveling tropical forcing with the observed OLR anomaly pattern.

5. Discussion and conclusions

In this study, the occurrence of blocking over the SE Pacific has been clearly linked by observational evidence and barotropic modeling experiments to the propagation of Rossby waves forced by tropical convection corresponding to observed mean OLR anomalies. The statistical methods employed in the observational analysis have focused on the location in the SE Pacific where the 500-hPa height variance maximizes. Our modeling results suggest that the location of this maximum may be due to its being the most favorable region for the channeling of Rossby wave energy given the observed mean flow.

Many of the observational results presented here refer to interannual variability and are strongly related to the ENSO cycle. However, similar wave propagation out of the Tropics has been shown by Mo and Higgins (1998) to be episodically associated with the 30–60-day Madden–Julian oscillation (MJO; Madden and Julian 1972), which acts on intraseasonal timescales. Variability in convection over the equatorial Pacific is ubiquitous over a wide range of timescales, presumably forcing continual adjustment processes and wave propagation between the tropical and extratropical troposphere. The OLR anomaly pattern shown in Fig. 8 seems to appear in most EOF analyses of tropical OLR and may be relevant to fluctuations on timescales from intraseasonal to interannual. A spectral analysis of the amplitude time series of the Fig. 8 OLR pattern showed a highly significant peak at around 2.5 yr and another broad peak in the 20–60-day range, consistent with ENSO and MJO variability. The SE Pacific blocking index exhibits con-

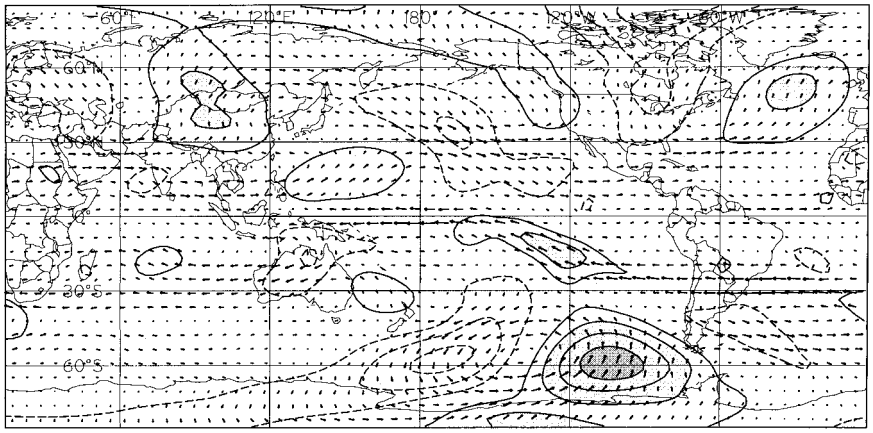

FIG. 16. As in Fig. 11 except after 12 days for the tropical forcing initially displaced 60° westward and propagating 5° eastward per day.

siderable spectral energy on the 2–4-yr timescale but has no strong spectral peaks on intraseasonal timescales.

We suggest the following explanation for the observations: Assume the background flow is changing on a longer timescale than that for Rossby wave propagation (about a week). A divergent circulation associated with the tropical OLR anomaly propagates toward the east, possibly associated with the MJO. This creates an eastward-moving source of Rossby waves, generated where the v component of the divergent circulation intersects the regions of large latitudinal gradient of vorticity, typically at the major jet streams. The Rossby wave source waxes and wanes in strength with the background jet intensity and possibly that of the tropical anomaly itself. The far-field wave response reflects this variation, plus any further interference by regions not favoring wave propagation. The maximum in variance in the SE Pacific results from the cooperative influence of all these effects.

Based on the above argument, the region of strong *low-frequency* circulation variability over the SE Pacific may be taken in part to reflect the mean pattern of variation over a large ensemble of such *high-frequency* Rossby wave passages, forced by continually varying tropical convection. Therefore, as stated in the introduction, the modulation of tropical convection by the ENSO cycle leads to a somewhat predictable modulation in the ensemble of SE Pacific blocking events over a season. However, the correct prediction of individual blocking events relies at least in part upon the correct initialization and simulation of the divergent tropical circulation associated with individual Rossby wave propagation events. Further work is required on this question, to isolate the observed tropical–extratropical linkages on different timescales.

The above analysis and modeling experiments are all linear and barotropic in nature. It is clear that nonlinear effects must come in to play, as the mean flow is modified by the perturbations associated with transient wave propagation (Andrews et al. 1987). However, we feel that the linear analysis shown here captures much of the relevant large-scale dynamics, in at least a qualitative sense.

Acknowledgments. The barotropic vorticity equation model code was kindly supplied by the atmospheric modeling group at Reading University, Reading, United Kingdom. We thank Lois Steenman-Clark, who helped adapt it to run locally. The NCEP–NCAR reanalysis dataset was provided by the Data Services Section at NCAR. Thanks to John Kidson, Kingtse Mo, David Karoly, and one anonymous reviewer for helpful comments on earlier drafts of this paper. This research was funded by the New Zealand Foundation for Research, Science and Technology under Contract CO1628.

REFERENCES

Ambrizzi, T., and B. J. Hoskins, 1997: Stationary Rossby-wave propagation in a baroclinic atmosphere. *Quart. J. Roy. Meteor. Soc.,* **123,** 919–928.

Andrews, D. G., J. R. Holton, and C. B. Leovy, 1987: *Middle Atmosphere Dynamics.* International Geophysics Series, Vol. 40, Academic Press, 489 pp.

Bretherton, C. S., C. Smith, and J. M. Wallace, 1992: An intercomparison of methods for finding coupled patterns in climate data. *J. Climate,* **5,** 541–560.

Craddock, J. M., and C. R. Flood, 1969: Eigenvectors for representing the 500 mb geopotential surface over the Northern Hemisphere. *Quart. J. Roy. Meteor. Soc.,* **95,** 576–593.

Dole, R. M., 1986: The life cycles of persistent anomalies and blocking over the North Pacific. *Advances in Geophysics,* Vol. 29, Academic Press, 31–69.

Hoerling, M. P., A. Kumar, and M. Zhong, 1997: El Nino, La Nina, and the nonlinearity of their teleconnections. *J. Climate,* **10,** 1769–1786.

Horel, J. D., and J. M. Wallace, 1981: Planetary-scale atmospheric phenomena associated with the Southern Oscillation. *Mon. Wea. Rev.,* **109,** 813–829.

Hoskins, B. J., and D. J. Karoly, 1981: Steady linear response of a spherical atmosphere to thermal and orographic forcing. *J. Atmos. Sci.,* **38,** 1179–1196.

——, and T. Ambrizzi, 1993: Rossby wave propagation on a realistic longitudinally varying flow. *J. Atmos. Sci.,* **50,** 1661–1671.

Jin, F., and B. J. Hoskins, 1995: The direct response to tropical heating in a baroclinic atmosphere. *J. Atmos. Sci.,* **52,** 307–319.

Jolliffe, I. T., 1986: *Principal Component Analysis.* Springer-Verlag, 271 pp.

Kalnay, E., and Coauthors, 1996: The NCEP/NCAR 40-Year Reanalysis Project. *Bull. Amer. Meteor. Soc.,* **77,** 437–471.

Karoly, D. J., 1983: Rossby wave propagation in a barotropic atmosphere. *Dyn. Atmos. Oceans,* **7,** 111–125.

——, R. A. Plumb, and M. Ting, 1989: Examples of the horizontal propagation of quasi-stationary waves. *J. Atmos. Sci.,* **46,** 2802–2811.

Kayano, M. T., V. E. Kousky, and J. E. Janowiak, 1995: Outgoing longwave radiation biases and their impacts on empirical orthogonal function modes of interannual variability in the tropics. *J. Geophys. Res.,* **100** (D2), 3173–3180.

Kidson, J. W., 1999: Principal modes of Southern Hemisphere low-frequency variability obtained from NCEP–NCAR reanalyses. *J. Climate,* **12,** 2806–2828.

Kiladis, G. N., and K. C. Mo, 1998: Interannual and intraseasonal variability in the Southern Hemisphere. *Meteorology of the Southern Hemisphere, Meteor. Monogr.,* No. 49, Amer. Meteor. Soc., 307–336.

Madden, R. A., and P. Julian, 1972: Description of global scale circulation cells in the tropics with a 40–50 day period. *J. Atmos. Sci.,* **29,** 1109–1123.

Mo, K. C., and R. W. Higgins, 1998: The Pacific–South American modes and the tropical intraseasonal oscillation. *Mon. Wea. Rev.,* **126,** 1581–1596.

Mullen, S. L., 1987: Transient eddy forcing of blocking flows. *J. Atmos. Sci.,* **44,** 3–22.

Nakamura, H., and J. M. Wallace, 1993: Synoptic behavior of baroclinic eddies during the blocking onset. *Mon. Wea. Rev.,* **121,** 1892–1903.

——, M. Nakamura, and J. L. Anderson, 1997: The role of high- and low-frequency dynamics in blocking formation. *Mon. Wea. Rev.,* **125,** 2074–2093.

North, G. R., T. L. Bell, and R. F. Cahalan, 1982: Sampling errors in the estimation of empirical orthogonal functions. *Mon. Wea. Rev.,* **110,** 699–706.

Parker, D. E., P. D. Jones, C. K. Folland, and A. Bevan, 1994: Interdecadal changes of surface temperature since the late nineteenth century. *J. Geophys. Res.,* **99,** 14 373–14 399.

Plumb, R. A., 1985: On the three-dimensional propagation of stationary waves. *J. Atmos. Sci.*, **42,** 217–229.
Rasmusson, E. M., and K. C. Mo, 1993: Linkages between 200-mb tropical and extratropical circulation anomalies during the 1986–1989 ENSO cycle. *J. Climate*, **6,** 595–616.
Renwick, J. A., 1998: ENSO-related variability in the frequency of South Pacific blocking. *Mon. Wea. Rev.*, **126,** 3117–3123.
——, and J. M. Wallace, 1995: Predictable anomaly patterns and the forecast skill of Northern Hemisphere wintertime 500-mb height fields. *Mon. Wea. Rev.*, **123,** 2114–2131.
——, and ——, 1996a: The influence of sampling variability upon model output error statistics. *Mon. Wea. Rev.*, **124,** 1981–1991.
——, and ——, 1996b: Relationships between North Pacific wintertime blocking, El Niño, and the PNA pattern. *Mon. Wea. Rev.*, **124,** 2071–2076.
Sardeshmukh, P. D., and B. J. Hoskins, 1988: The generation of global rotational flow by steady idealized tropical divergence. *J. Atmos. Sci.*, **45,** 1228–1251.
Shutts, G. J., 1983: The propagation of eddies in diffluent jet streams: Eddy vorticity forcing of blocking flow fields. *Quart. J. Roy. Meteor. Soc.*, **109,** 737–761.
Tibaldi, S., E. Tosi, A. Navarra, and L. Pendulli, 1994: Northern and Southern Hemisphere seasonal variability of blocking frequency and predictability. *Mon. Wea. Rev.*, **122,** 1971–2003.
Trenberth, K. E., 1997: The definition of El Niño. *Bull. Amer. Meteor. Soc.*, **78,** 2771–2777.
Tyrrell, G. C., D. J. Karoly, and J. L. McBride, 1996: Links between tropical convection and variations of the extratropical circulation during TOGA COARE. *J. Atmos. Sci.*, **53,** 2735–2748.